

Hard X-ray photoelectron spectroscopy on buried, off-stoichiometric $\text{Co}_x\text{Mn}_y\text{Ge}_z$ ($x : z = 2 : 0.38$) Heusler thin films.

Siham Ouadi, Gerhard H. Fecher,* Stanislav Chadov, and Claudia Felser

Max Planck Institute for Chemical Physics of Solids, D-01187 Dresden, Germany

Benjamin Balke and Xenia Kozina

Institut für Anorganische und Analytische Chemie,

Johannes Gutenberg - Universität, 55099 Mainz, Germany

Tomoyuki Taira and Masafumi Yamamoto

Division of Electronics for Informatics,

Hokkaido University, Sapporo 060-0814, Japan.

(Dated: October 2, 2012)

Abstract

Fully epitaxial magnetic tunnel junctions (MTJs) with off-stoichiometric Co_2 -based Heusler alloy shows a intense dependency of the tunnel magnetoresistance (TMR) on the Mn composition, demonstrating giant TMR ratios of up to 1995% at 4.2 K for ¹. This work reports on the electronic structure of non-stoichiometric $\text{Co}_x\text{Mn}_y\text{Ge}_z$ thin films with a fixed Co/Ge ratio of $x : z = 2 : 0.38$. The electronic structure was investigated by high energy, hard X-ray photoelectron spectroscopy combined with first-principles calculations. The high-resolution measurements of the valence band of the non-stoichiometric $\text{Co}_x\text{Mn}_y\text{Ge}_z$ films close to the Fermi energy indicate a shift of the spectral weight compared to bulk Co_2MnGe . This is in agreement with the changes in the density of states predicted by the calculations. Furthermore it is shown that the co-sputtering of Co_2MnGe together with additional Mn is an appropriate technique to adjust the stoichiometry of the $\text{Co}_x\text{Mn}_y\text{Ge}_z$ film composition. The resulting changes of the electronic structure within the valence band will allow to tune the magnetoresistive characteristics of $\text{Co}_x\text{Mn}_y\text{Ge}_z$ based tunnel junctions as verified by the calculations and photoemission experiments.

PACS numbers: 79.60.i, 79.60.Jv, 85.75.d, 73.50.-h

Keywords: Photoelectron spectroscopy, Electronic structure, Magnetic tunnel junctions, Heusler compounds

I. INTRODUCTION

Nowadays, Co_2 based Heusler compounds are successfully used as ferromagnetic electrodes providing a spin polarized electrical current in tunneling magnetoresistive (TMR) junctions²⁻⁴. To produce high performance spintronic devices with Co_2 based Heusler thin films as ferromagnetic electrodes, it is necessary to clarify the dependence of the magnetoresistive characteristics on the stoichiometry of the Heusler film electrode and its impact on the selection of materials for TMR devices. However, very little is known about the electronic structure of non-stoichiometric Heusler compounds.

Furthermore, partially substitution of one of the elements in the ternary Heusler $T_2T'M$ (where, T, T' is transition metals and M main group element) can be used to design new materials with predictable properties^{5,6}, such as tuning the Fermi energy in to the middle of the minority band gap⁷. The partially substitution of the elements in $T_2T'M$ leads to substitutional quaternary alloys of the type $T_2T'_{1-x}T''_xM$ or $T_2T'M_{1-x}M'_x$. The quaternary alloy $\text{Co}_2\text{Cr}_{0.6}\text{Fe}_{0.4}\text{Al}$ has attracted emerged interest as potential material for magnetoelectronics, due to the large MR^{8,9}. The band structure calculations confirmed the halfmetallic state of this compound in the ordered $L2_1$ structure^{5,6,8}. Recently, several groups developed fully epitaxial magnetic tunnel junctions (MTJs) based on $\text{Co}_2\text{Cr}_{0.6}\text{Fe}_{0.4}\text{Al}$ as a lower electrode and a MgO tunnel barrier¹⁰⁻¹². However, a disorder of the structure results in a strongly reduced magnetic moment as well as a loss of the half-metallic character^{13,14}.

Co_2MnZ ($Z = \text{Si}, \text{Ge}, \text{Sn}$) are representatives of Heusler compounds with a specific electronic band structure providing a pronounced dependence of its transport properties on the orientation of the electron spin^{15,16}. Structural and magnetic properties of Co_2MnSi were reported for films and single crystals^{17,18} and the compound was suggested to be suitable for magnetic tunnel junctions (MTJs)^{2,19,20}. A high TMR ratio of 179% at room temperature (RT) and 683% at 4.2 K was revealed by Ishikawa and coworkers². The Substitution of Fe by Mn in $\text{Co}_2\text{Fe}_x\text{Mn}_{1-x}\text{Si}$ shows a dependency of half-metallicity and Gilbert damping constant on the composition x ^{21,22}. Recently, anisotropic magnetoresistance (AMR) effect was systematically investigated in epitaxially grown $\text{Co}_2\text{Fe}_x\text{Mn}_{1-x}\text{Si}$ Heusler films with respect to Fe composition x and the annealing temperature²³. It was shown that the AMR effect can be an indicator of half-metallicity.

An appropriate alternative to Co_2MnSi is the isovalent Co_2MnGe with 29 valence elec-

trons in the primitive cell. Recently, Co_2MnGe was investigated in greater detail by theoretical and experimental methods in order to prove the half metallic ferromagnetic character, as well as their crystallographic structure, mechanical and transport properties²⁴. This compound is of interest for spintronic applications because it combines high Curie temperature (905 K)²⁵, high magnetic moment ($5 \mu_B$)²⁶, and coherent growth on top of semiconductors^{27,28}. The non-stoichiometric Co_2MnGe was successfully used to produce magnetic tunnel junctions^{29–31}. Hakamata and coworkers fabricated epitaxial MTJs with a Co-rich Co_2MnGe film and reached relatively low TMR ratios of 83% at RT and 185% at 4.2 K³². Thereafter, Taira and coworkers investigated the influence of the annealing temperature on the performance of the MTJs. They achieved a significant increase of the TMR up to 160% at RT (376% at 4.2 K) by annealing at 500°C^{33,34}. This increase was explained in terms of the increase in the interfacial spin polarization at the Fermi level associated with the change in the spin-dependent interfacial density of states. On the other hand, the effect of defects in $\text{Co}_2\text{Mn}_\beta\text{Ge}_\delta$ and $\text{Co}_2\text{Mn}_\alpha\text{Si}$ films on the TMR ratio was extensively studied in Reference³¹ where a strong dependence on the composition and Mn content was observed. A high TMR ratio of 650% at 4.2 K and 220% at RT for $\text{Co}_2\text{Mn}_\beta\text{Ge}_\delta$ with $\beta=1.40$ was found. The highest TMR ratios for Heusler based MTJs of 1135% at 4.2 K and 236% at RT was achieved for Mn-rich $\text{Co}_2\text{Mn}_\alpha\text{Si}$ electrodes with $\alpha=1.29$. It was suggested that detrimental Co_{Mn} antisites can be suppressed by preparing the films with a Mn-rich composition.

The present work reports on the theoretical background and experimental studies of the electronic structure of non-stoichiometric $\text{Co}_2\text{Mn}_\beta\text{Ge}_\delta$. *ab-initio* electronic structure calculations are used to verify the range of existence of the half-metallic ferromagnetic behavior. High resolution photoelectron spectroscopy of the core levels and valence states of buried $\text{Co}_2\text{Mn}_\beta\text{Ge}_\delta$ films was used to explore the electronic structure in comparison to the theoretical predictions. Hard X-ray photoelectron spectroscopy (HAXPES) was previously shown to be a bulk sensitive probe of the electronic structure^{35–39}. The use of high-brilliance high-flux X-rays from the third-generation synchrotron radiation sources results the emission of electrons having high kinetic energies, in turn leading to a high probing depth because of the increased electron mean free path⁴⁰. Recently, several studies using high-resolution HAXPES have been realized. The electronic structure of solids like valence transitions in bulk systems⁴¹ as well as multilayer systems⁴⁰ and the valence band of buried thin films³⁵ have been investigated. Newly, The use of polarized light in combination with HAXPES enables

the analysis of the symmetry of bulk electronic states⁴² as well as the magnetic properties of buried layers⁴³. HAXPES was used in the present work to study buried $\text{Co}_2\text{Mn}_\beta\text{Ge}_\delta$ films underneath MgO/AlO_x capping layers. The study of core level photoelectron spectra of the buried Heusler thin films gives information on the electronic structure and the chemical composition of these films.

II. EXPERIMENT

For the present study, special multi-component thin film arrangements were produced that corresponded to a half of a magnetic tunnel junction as used in TMR devices (see Figure 1). In particular the free electrode was modeled. The fabricated sample layer structure was as follows: $\text{MgO}(001)$ substrate (0.5 mm) / MgO buffer layer (10 nm) / $\text{Co}_2\text{Mn}_\beta\text{Ge}_\delta$ (30 nm or 50 nm) / MgO barrier (t_{MgO}) / AlO_x (1 nm) cap. $t_{\text{MgO}} = 2$ nm and 20 nm were chosen for the thickness of the MgO layer. The topmost AlO_x was used for protection of the hygroscopic MgO layer during contact with air. The sample structure is sketched in Figure 1.

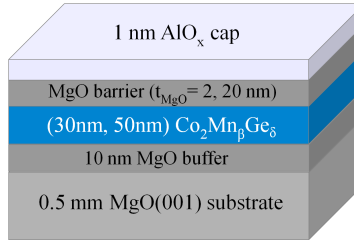


FIG. 1. Schematic sample structure.

Each layer in the sample layer structure was successively deposited in an ultrahigh vacuum chamber (base pressure: about 6×10^{-8} Pa) through the combined use of magnetron sputtering for Co_2MnGe and Al , and electron beam evaporation for MgO . The fabrication procedure was the same as in previous works^{2,44}. The thin films were deposited at 300 K and subsequently annealed in situ at 500°C for 15 min. Co-sputtering from an additional Mn target was applied to vary the Mn content of the $\text{Co}_2\text{Mn}_\beta\text{Ge}_\delta$ thin films. X-ray diffraction revealed that the $\text{Co}_2\text{Mn}_\beta\text{Ge}_\delta$ films have a dominating $L2_1$ crystalline structure. The resulting Co_2MnGe layers used in the photoemission study were estimated to be non-stoichiometric with the compositions of 2 : 1.03 : 0.38, 2 : 0.77 : 0.42, and 2 : 0.67 : 0.38 (see Reference³¹).

The MgO barrier was deposited at 300 K. The AlO_x cap was prepared by exposing the sputter-deposited Al layer to an O_2 atmosphere of $\approx 1 \times 10^5$ Pa for 2 hours.

The precise occupation probability for each particular site of an assumed $L2_1$ structure is unknown although the relative amounts of constituents are well-defined. For this reason we will use the composition formula³¹ derived from theoretical estimations⁴⁵ of the defect formation energies, using the permanent ratio of Co:Mn:Ge as $2 : \beta : 0.38$. Firstly, it is assumed that the Co-Mn-Ge alloy series basically does not contain vacancies. The Ge deficiency is compensated by Mn (Mn_{Ge} antisites). The lack of Mn in its native octahedral position is backfilled by Co_{Mn} antisites. Further, the lack of Co in the tetrahedral sites is compensated by Mn_{Co} antisites. This leads to the following compositions for $\delta = 0.38$: $\text{Co}_2(\text{Mn}_{1-x}\text{Co}_x)(\text{Ge}_{1-y}\text{Mn}_y)$ for Mn deficit ($\beta \leq 1.62$) and $(\text{Co}_{1-x/2}\text{Mn}_{x/2})_2\text{Mn}(\text{Ge}_{1-y}\text{Mn}_y)$ for Mn excess ($\beta \geq 1.62$). For $\delta = 0.38$, the x and y antisite concentrations as function of the Mn content parameter β are determined by the relations:

- $2 + x : 1 - x + y : 1 - y = 2 : \beta : 0.38$ ($\beta \leq 1.62$);
- $2 - x : 1 + x + y : 1 - y = 2 : \beta : 0.38$ ($\beta \geq 1.62$),

This corresponds to the experiments reported in Reference³¹.

In the regular $L2_1$ structure of the X_2YZ Heusler compounds, the atoms occupy the Wyckoff positions 8a (X_2) (T_d), 4a (Y) (O_h), and 4b (Z) (O_h) of the primitive cell with $Fm\bar{3}m$ symmetry (space group 225). Table I summarizes the site occupations of the primitive cell for the different β values. $\beta = 0.28\bar{6}$ corresponds to a DO_3 structure according to $\text{Co}_3(\text{Mn}_{0.43}\text{Ge}_{0.57})$. It should be noted that for compositions with $\text{Mn} : \text{Co} > 2$ ($\beta > 1.62$) a Y -type structure with $F\bar{4}3m$ symmetry (space group 216) can be expected where the 8c position of the $L2_1$ structure is split into 4c and 4d such that all sites (4a-4d) have T_d symmetry. In that case Mn may occupy 4a and 4c whereas Co and Ge are distributed on 4b and 4d. Further, it is known that the binary alloys $\text{Co}_{0.5}\text{Mn}_{0.5}$ ⁴⁶ or $\text{Co}_{0.87}\text{Ge}_{0.13}$ ⁴⁷ crystallize in fcc lattices with random site occupation and similar lattice parameters. Therefore, other types of disorder or site occupations cannot be excluded. Due to the similar scattering amplitudes of the constituents, however, X-ray diffraction is not unambiguous in the structure determination.

TABLE I. Selected site occupations of the primitive cell for the different β values of $\text{Co}_2\text{Mn}_\beta\text{Ge}_{0.38}$. The ratio of the Co:Ge content is fixed at 2 : 0.38 and all sites are completely occupied. Ge is placed exclusively on the 4b position. The site occupation for the compound with Co:Ge = 2 : 0.42 and the original $L2_1$ structure are included for completeness.

Composition	β	Co (8c)	Co (4a)	Mn (4a)	Mn (8c)	Ge (4b)	Mn (4b)
$\text{Co}_3\text{Mn}_{0.43}\text{Ge}_{0.57}$	0.28667	100%	100%	0	0	57%	43%
$\text{Co}_{2.62}\text{Mn}_{0.88}\text{Ge}_{0.49}$	0.67	100%	62%	38%	0	50%	50%
$\text{Co}_{2.5}\text{Mn}_{0.97}\text{Ge}_{0.53}$	0.77, $\delta = 0.42$	100%	51%	49%	0	52%	48%
$\text{Co}_{2.37}\text{Mn}_{1.18}\text{Ge}_{0.45}$	1	100%	37%	63%	0	45%	55%
$\text{Co}_{2.35}\text{Mn}_{1.21}\text{Ge}_{0.44}$	1.03	100%	35%	65%	0	45%	55%
$\text{Co}_2\text{Mn}_{1.62}\text{Ge}_{0.38}$	1.62	100%	0	100%	0	38%	62%
$\text{Co}_{1.82}\text{Mn}_{1.82}\text{Ge}_{0.35}$	2	91%	0	100%	9%	35%	65%
$\text{Co}_{1.68}\text{Mn}_2\text{Ge}_{0.32}$	2.38	84%	0	100%	16%	32%	68%
Co_2MnGe	$L2_1$	100%		100%		100%	

III. CALCULATIONS OF THE ELECTRONIC STRUCTURE

To understand the electronic structure of the non stoichiometric compounds, first-principles calculations were performed using the KKR (Korringa-Kohn-Rostoker) Green's function method as implemented in the Munich SPR-KKR (spin-polarized relativistic) package^{48,49}. The chemical disorder is treated by the coherent potential approximation (CPA)^{50,51}. Exchange and correlation are treated within the local spin density approximation (LSDA) using the parametrization of Vosko, Wilk and Nussair⁵². The full symmetry potential method was used in order to account for the non spherical character of the atomic potentials in solids that is rather significant in Heusler compounds. The k -integration mesh was set to a size of $(22 \times 22 \times 22)$ during the selfconsistent cycles resulting in 328 points in the irreducible wedge of the Brillouin zone. The expansion in spherical harmonics up to $l_{\text{max}} = 3$ (f -electrons) was found to be numerically sufficient. The calculations were performed for a disordered $L2_1$ structure to account for the composition dependence. The site occupations for the different compositions are explained in detail in Section II.

The results of the electronic structure calculations are discussed in the following. It is

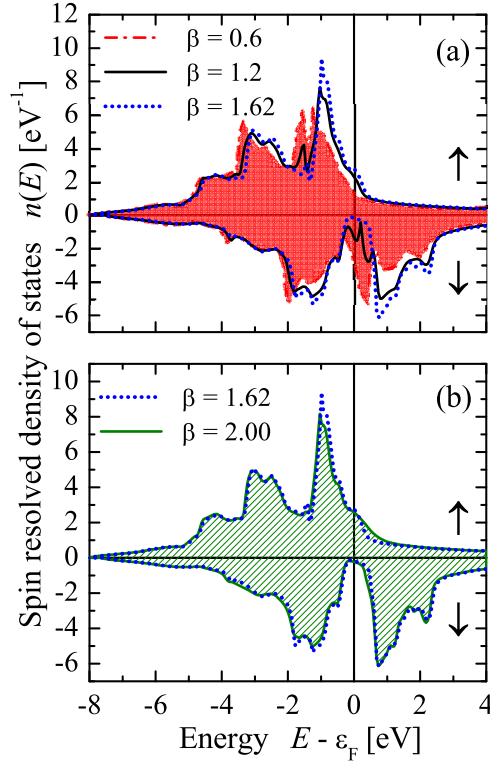


FIG. 2. (color online) Spin-resolved DOS calculated for (a) Mn-deficient ($\beta \leq 1.62$) series, (b) Mn-excessive ($\beta = 1.62, 2.0$) series. Minority states (\downarrow) are shown on a negative scale.

obvious from the comparison of the density of state (Figures 2(a) and (b)) that the most significant factor influencing the electronic properties is the formation of Co_{Mn} -antisites in the Mn-poor regime ($\beta < 1.62$). In full analogy to Co-Mn-Si alloy systems^{45,53}, Co_{Mn} -antisites introduce impurity-like states (shown separately in Figure 6) inside of the half-metallic band gap that seriously destroy the spin-polarization (see Figure 4: $\beta < 1.62$). In general, the spin polarisation at the Fermi energy is defined by:

$$P(\epsilon_F) = \frac{v_{\uparrow}^x n_{\uparrow}(\epsilon_F) - v_{\downarrow}^x n_{\downarrow}(\epsilon_F)}{v_{\uparrow}^x n_{\uparrow}(\epsilon_F) + v_{\downarrow}^x n_{\downarrow}(\epsilon_F)}, \quad (1)$$

where v_{\uparrow} and v_{\downarrow} are the Fermi velocities for majority and minority electrons, respectively. In photoemission one has $x = 0$ such that the spin polarisation is purely given by the majority (n_{\uparrow}) and minority (n_{\downarrow}) densities. The situation is, however, different for the TMR wherefore the values can not be compared directly but only their trend. It is worthwhile to note that in halfmetallic ferromagnets one has $P(\epsilon_F) = 1$ independent of the method.

The total magnetic moment in the Mn-deficient alloy strongly deviates from the Slater-

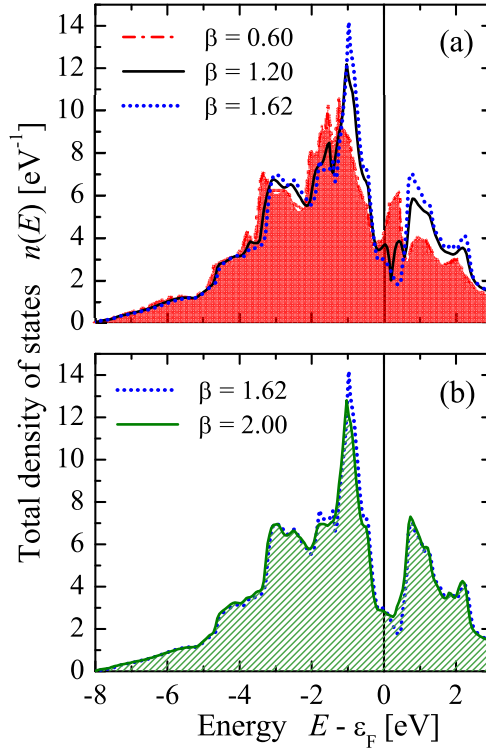


FIG. 3. (color online) Total DOS (sum of both spin channels) calculated for (a) Mn-deficient ($\beta \leq 1.62$) (b) Mn-excess ($\beta = 1.62, 2.0$).

Pauling rule (Figure 5(a): $\beta < 1.62$). This reasonably agrees with the measured TMR ratio and magnetic moments³¹.

In contrast, the excess of Mn (which result in a formation of Mn_{Co} antisites) does not influence the half-metallic gap noticeable (Figure 2(b)). The system remains nearly half-metallic. This restores the Slater-Pauling behavior of the total magnetic moment (Figure 5(a): $\beta > 1.62$). The slightly reduced value of the spin-polarization for $\beta \geq 1.62$ is mainly caused by Mn_{Ge} antisites permanently present in the whole series. This is also reflected in a slightly reduced value of the total magnetic moment compared to the Slater-Pauling rule.

As it follows from the calculated atomic-resolved magnetic moments shown in Figure 5(b), the total magnetization is mainly controlled by the amount of Co_{Mn} and Mn_{Co} antisites. For the Mn-deficient system the strong moment at the Mn atom (about $3 \mu_{\text{B}}$) in the octahedral position is accompanied by the lower moment of the Co_{Mn} antisite (about $1.9 \mu_{\text{B}}$). This is the reason for the violation of the Slater-Pauling rule. On the other hand, all possible

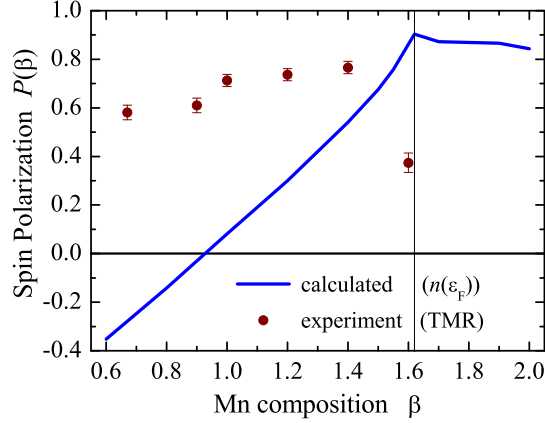


FIG. 4. Spin-polarization P at the Fermi energy calculated as a function of Mn composition β . Compared are the values from ab-initio calculations to experimental values calculated from the TMR measured at 4.2 K (see Ref.:³¹) using $P_{TMR} = TMR/(TMR + 2)$. The vertical line assigns $\beta = 1.62$.

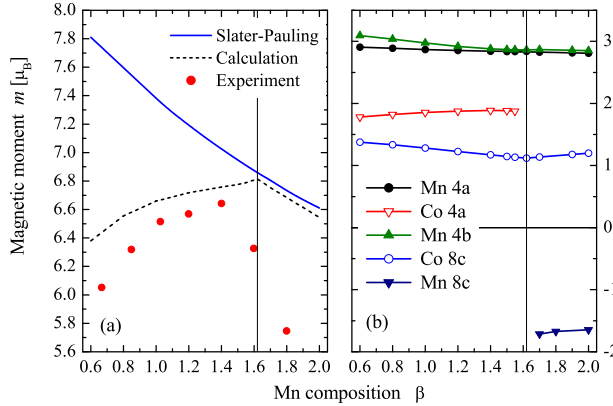


FIG. 5. (color online) (a) Total magnetic moments calculated as a function of Mn composition β (experimental data from³¹); (b) Calculated partial magnetic moments. (See Table I for the notation of the Wyckoff positions 4a, 4b, 8c and their site occupations; vertical lines are at $\beta = 1.62$.)

Mn permutations always result into half-metallic contributions. For the Mn-excessive alloys, formation of the Mn_{Co} antisites at tetrahedral positions exhibit a negative moment of about $-1.7 \mu_B$. The ferrimagnetic coupling between the regular Mn atom and the Mn_{Co} antisite appears because they are nearest neighbors. Obviously, the magnetic interaction between neighboring Co atoms is smaller when part of them occupies Co_{Mn} antisites due to the

smaller extend of the d -wave functions.

From the comparison of the total (spin-integrated) density of states (see Figure 3) and the photoelectron spectra (Figure 10), it was found that the Mn e_g states decrease with decreasing Mn content. For the Mn-poor alloys the minimum of the density of state at the Fermi energy is destroyed by the appearance of Co_{Mn} antisites. With increasing the Mn content the model system behaves as a half-metal following the Slater-Pauling scenario. The rapid decrease of the measured magnetization³¹ above $\beta = 1.4$ (see Figure 5(a)) may be attributed to difference types of disorder including possible structural distortions in thin films.

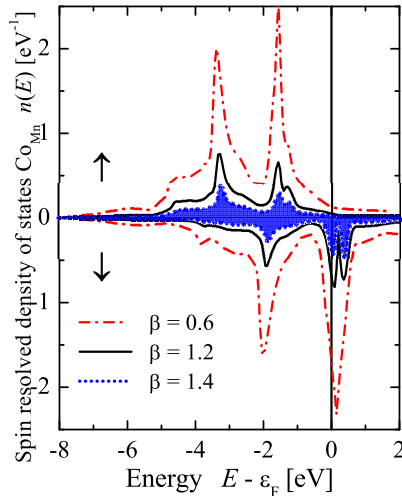


FIG. 6. (color online) Spin-resolved DOS of Co_{Mn} (Co antisites) for Mn-deficient regime ($\beta < 1.62$). Minority states (\downarrow) are shown on a negative scale.

IV. HARD X-RAY PHOTOELECTRON SPECTROSCOPY

The HAXPES experiments were performed at the undulator beamlines BL15XU and BL47XU of SPring-8. At BL15XU, the photon energy was fixed at 5.9469 keV using a Si(111) double crystal monochromator (DCM) and a the 333 reflection of a Si channel-cut post monochromator. At BL47XU, the photon energy was fixed at 7.9382 keV using a Si(111) DCM and a Si(444) channel-cut post monochromator. The photo-emitted electrons were analyzed for their kinetic energy and detected by a hemispherical analyzer (VG Scienta R4000). The overall energy resolution (monochromator plus analyzer) was set to 250 meV,

as verified by spectra of the Au valence band at the Fermi energy (ϵ_F). Additionally, spectra close to the Fermi energy were taken with a total energy resolution of 150 meV. The angle between the electron spectrometer and photon propagation is fixed at 90° in all experiments. A near normal emission ($\theta = 2^\circ$) detection angle was used resulting in an angle of photon incidence of $\alpha = 88^\circ$. The measurements were taken at sample temperatures of 20 K and 300 K.

A. Core level spectroscopy

Hard X-ray core level spectra were measured on $\text{Co}_2\text{Mn}_\beta\text{Ge}_\delta$ films with different compositions to investigate the influence of the off-stoichiometry on the spin orbit splitting as well as the exchange interaction of the unpaired valence electrons with the core holes.

Figures 7(a) and (b) compare the hard X-ray Co $2p$ and Mn $2p$ core level spectra of the non-stoichiometric $\text{Co}_2\text{Mn}_\beta\text{Ge}_\delta$ films covered with 2 nm MgO. The spectra were taken at room temperature with an excitation energy of about 8 keV. Concentrating on the Co $2p$ region, Figure 7(a) illustrates a spin-orbit splitting between the Co $2p_{3/2}$ and $2p_{1/2}$ states of about 14.86 eV. There is no remarkable change of the splitting or line width detected for the different non-stoichiometric films. All spectra exhibit a satellite at about 4 eV below the center of the $2p_{3/2}$ main line. Such satellites were also observed in the previous work^{36,37}. The satellite emerges from the interaction of the $2p$ core hole with the partially filled d valence bands. To clarify the detailed origin of the satellite structure, theoretical calculations are required that treat the details of the exchange interaction between the Co $3d$ electron occupation (in other words, the band structure) and $2p$ core hole states. At the $2p_{1/2}$ state it is only seen weakly as a tail at the low energy side due to shorter lifetime of the core hole compared with the $2p_{3/2}$ state.

Figure 7(b) shows the Mn $2p$ photoelectron spectra for the buried Heusler thin films $\text{Co}_2\text{Mn}_{1.03}\text{Ge}_{0.38}$ and $\text{Co}_2\text{Mn}_{0.67}\text{Ge}_{0.38}$. The peak intensity of the spin-orbit split $2p$ states of the Mn-rich film $\text{Co}_2\text{Mn}_{1.03}\text{Ge}_{0.38}$ were slightly higher than those with less Mn. This is in agreement with the estimated composition of the films. In analogy to the Co $2p$ spectra, the Mn $2p$ core level shows the spin-orbit splitting of about 12.1 eV. Different to the Co $2p$ spectra, the multiplet splitting of the Mn $2p_{3/2}$ state was clearly revealed (see inset in Figure 7(b)). It was shown theoretically and experimentally for the case of Mn that the

Coulomb interaction of the $2p$ core hole and the $3d$ valence electrons leads to the splitting of the Mn $2p_{3/2}$ level into several main sublevels⁵⁴ caused by existence of more than one possible final ionic state during ejection of an electron from the p shell. The effect of the exchange interaction between $2p$ core hole and the partially filled d -bands is less pronounced at the $2p_{1/2}$ state but still clearly detectable. The small influence of the composition on the Mn $2p$ derived multiplet is in agreement with the electronic structure calculations where the localized Mn d bands and the magnetic moment at Mn are stable against variation of the composition. This finding underlines the localized character of the Mn valence d electrons.

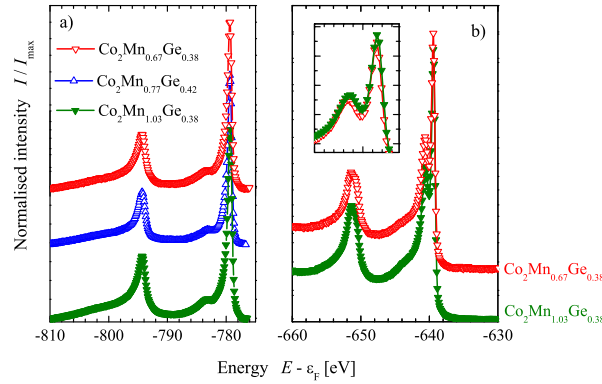


FIG. 7. HAXPES spectra of the Co $2p$ (a) and Mn $2p$ (b) core level of $\text{Co}_2\text{Mn}_\beta\text{Ge}_\delta$ films. The spectra are taken at room temperature. The excitation energy was set to $h\nu = 7.9382$ keV. The inset in (b) shows the details of the Mn $2p_{3/2}$ peak on an enlarged scale.

Figure 8 compares the hard X-ray photoelectron spectra of the shallow core levels with low binding energy of the 50 nm thick $\text{Co}_2\text{Mn}_{0.77}\text{Ge}_{0.42}$ layer buried underneath MgO/AlO_x with different thicknesses of the MgO interlayer. The intensity ratios of the core level $I_{2s}^{\text{Mg}}/I_{3s}^{\text{Ge}}$ of the films covered with 2 nm or 20 nm thick MgO are 0.95 or 16.45, respectively. This strong increase is caused by the increase of the emission from the thick MgO layer. The inset of Figure 8 shows the valence band of the covered thin films. The high intensity at -1.3 eV below ϵ_F is clearly resolved and agrees well with the bulk spectra (see also: Figures 9 and 10). The low lying s band below -8 eV is only seen for the film with the 2 nm thick MgO layer. This part, in addition to the lower parts of the p and d bands, is covered by the emission from the Mg $3s$ and O $2p$ states when the MgO film is 20 nm thick. This has been already reported for other Heusler compounds³⁵ and makes clear that the valence band

spectra close to the Fermi energy are not influenced by the insulating layers above.

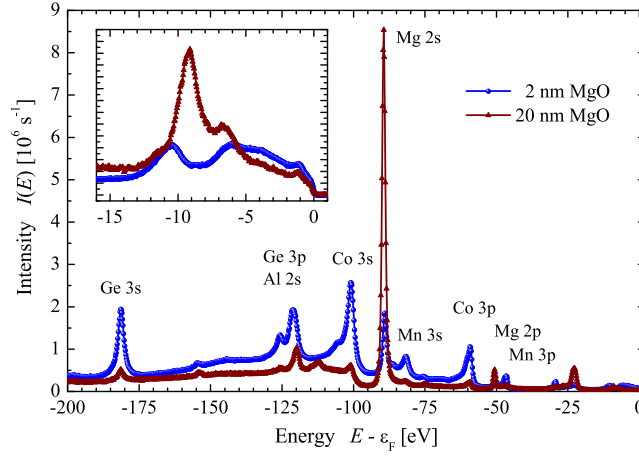


FIG. 8. HAXPES spectra of the shallow core states of buried $\text{Co}_2\text{Mn}_{0.77}\text{Ge}_{0.42}$ thin films. The spectra with different thickness of the MgO layer (2 nm and 20 nm) are compared. The excitation energy was set to 7.9392 keV. The small peak at about -25 eV is due to the O 2s excitation. The inset compares the valence band spectra for different MgO thickness.

B. Valence band spectroscopy

Figure 9 compares the valence band spectra of the non-stoichiometric $\text{Co}_2\text{Mn}_\beta\text{Ge}_\delta$ films to stoichiometric bulk Co_2MnGe . The main features of the valence band of the thin films agree well with that of the bulk sample. The intense, broad band at about -10.5 eV is observed for the buried films as well as for the bulk sample. This band is related to Ge a_{1g} (s) states and is separated from the remaining valence bands by the sp hybridization gap at around -8.5 eV. This low lying band gap is characteristic for well ordered Heusler compounds with $L2_1$ structure. This hybridization gap is well pronounced for the bulk sample, confirming the ordered structure. Additional features within the sp hybridization gap are seen in the spectra of the buried films. Partially, this intensity arises from the O 2p states of the oxide overlayers and thus a direct comparison to the *clean* bulk material is not straightforward. However, the difference in the spectral shapes between the films with altered composition one has the same overlayer and differences in the spectra can be considered as an evidence for the disorder rising up when changing the composition. The spectral shape above about -6 eV are not influenced by the MgO and AlO_x layers as already mentioned above. Overall,

the spectra of the $\text{Co}_2\text{Mn}_\beta\text{Ge}_\delta$ films show broadened structures compared to the spectrum of bulk Co_2MnGe . This broadening of the bands is explained by the disturbed translational periodicity due to the random site occupation or periodically unoccupied sites in the non-stoichiometric $\text{Co}_2\text{Mn}_\beta\text{Ge}_\delta$ films. The majority Mn t_{2g} states at about -3.9 eV, that are responsible for the localized magnetic moment at the Mn atoms, are much less pronounced in the non-stoichiometric films compared to stoichiometric Co_2MnGe . All the states far below ϵ_F influence mainly the magnetic but not directly the transport properties.

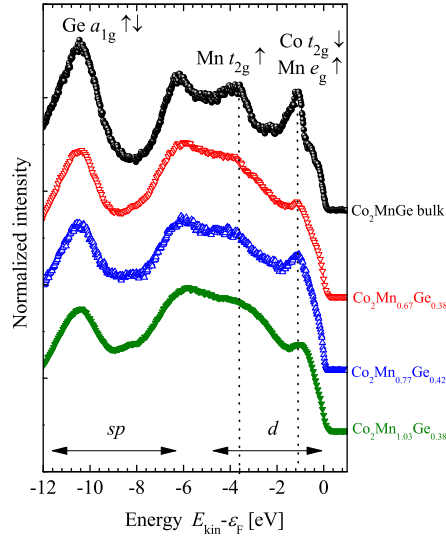


FIG. 9. Valence band spectra of the $\text{Co}_2\text{Mn}_\beta\text{Ge}_\delta$ films and Co_2MnGe bulk sample. The excitation energy was set to 7.9392 keV.

Most interesting with respect to the transport properties, in particular the use of the films in TMR devices, is the energy range close to the Fermi energy. The maximum in the density of the d states at -1.1 eV is clearly resolved in the spectra from all films and the intensity varies when Mn content is changed (see Figure 10). This maximum in the intensity arises from Co t_{2g} minority and Mn e_g majority states. Obviously, those states appear much stronger and sharper in the stoichiometric bulk sample pointing to their higher localization in the defect free sample. The intensity directly at ϵ_F is dominated by t_{2g} majority states that are mainly located in the Co_2 planes of the compound. The increase of the Mn content enhances the intensity of the highest majority d -band that is mainly responsible for the electronic transport properties. Such composition dependent behavior of the density of

states close to ϵ_F provides the possibility to tune the magnetoresistive characteristics of tunnel junctions by changing the composition of the $\text{Co}_2\text{Mn}_\beta\text{Ge}_\delta$ electrode, as was previously proposed in Reference³¹.

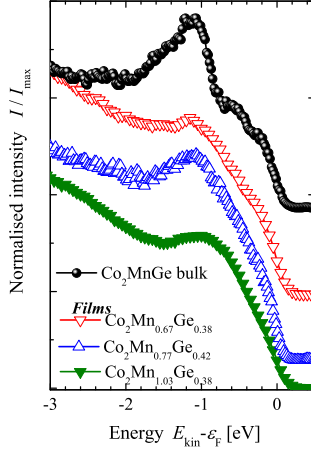


FIG. 10. Valence band spectra close to ϵ_F . The spectra are taken for Co_2MnGe bulk as well as thin $\text{Co}_2\text{Mn}_{1.03}\text{Ge}_{0.38}$, $\text{Co}_2\text{Mn}_{0.77}\text{Ge}_{0.42}$, and $\text{Co}_2\text{Mn}_{0.67}\text{Ge}_{0.38}$ films. The excitation energy was set to 7.9392 keV.

Figure 11 compares the valence band spectra on the buried $\text{Co}_2\text{Mn}_{0.77}\text{Ge}_{0.42}$ film taken with different photon energies of about 5.946 keV and 7.939 keV. The differences in the spectra are caused by the different weights of the partial cross-sections for s , p , and d electrons at different excitation energies²⁶. With increasing energies the cross-sections for d electron excitation decrease faster than those for s or p electrons. Therefore, the contribution from d electrons is more pronounced at lower energy photo-excitation. The observed shift of spectral weight towards the Fermi energy in the non-stoichiometric films compared to bulk Co_2MnGe is in agreement with the changes in the density of states predicted by the calculations.

Furthermore, the valence band spectra of the $\text{Co}_2\text{Mn}_{0.77}\text{Ge}_{0.42}$ thin films taken at room temperature and at 20 K are compared in Figure 12. No general changes in the electronic structure are observed in the spectra while changing temperature. At $T = 20$ K a small, additional peak appears that is caused by adsorbed carbon oxides on the surface of the samples while cooling. This observation provides evidence for the requirement on ultra high vacuum for HAXPES measurement even though this

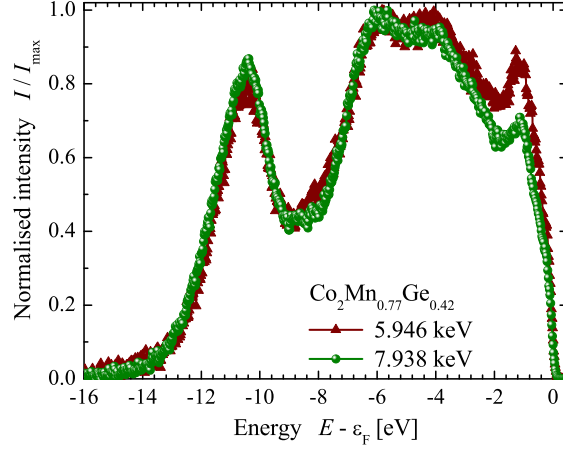


FIG. 11. Comparison of the valence band spectra of the $\text{Co}_2\text{Mn}_{0.77}\text{Ge}_{0.42}$ film excited by different photon energies (5.9469 keV and 7.9382 keV).

technique is bulk sensitive. Indeed, a massive contamination of the surface in the order of several layers will influence the HAXPES spectra.

Figure 12(b) shows a broadening of the spectra close to the Fermi energy. The broad spectral feature in the vicinity of the Fermi energy at 300 K compared to 20 K is caused by the temperature dependence of the Fermi-Dirac distribution. This observation is in agreement with reports showing that Co_2MnSi films do not exhibit temperature effects in photoelectron spectroscopy⁵⁵.

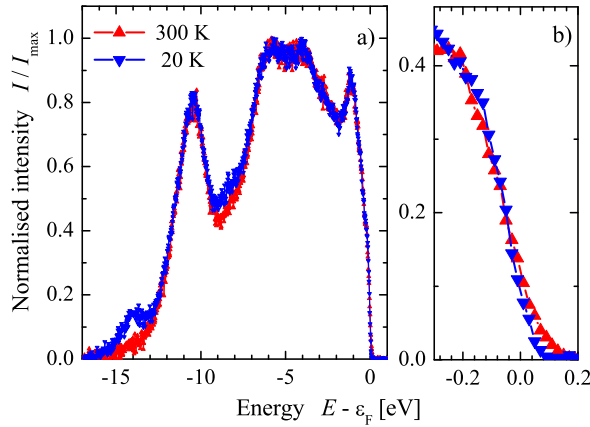


FIG. 12. Valence band spectra of $\text{Co}_2\text{Mn}_{0.77}\text{Ge}_{0.42}$ film. (a) compares the spectra measured at different temperatures ($h\nu = 5.9469$ keV). (b) shows the energy range close to the Fermi energy on an enlarged scale.

V. SUMMARY AND CONCLUSIONS

In summary, the electronic structure of off-stoichiometric $\text{Co}_2\text{Mn}_\beta\text{Ge}_\delta$ alloys was investigated by first-principles calculations and bulk sensitive photoelectron spectroscopy on thin films. The electronic structure calculations demonstrate that the magnetic moments of Co and Mn atoms (including the antisites) are nearly independent of the stoichiometry. This finding is in agreement with the core level photoelectron spectra where no differences in the multiplet splitting of the Mn $2p$ states was observed for different compositions.

The formation of Co_{Mn} antisites was found to be the most destructive depolarizing mechanism. Corresponding results for the Mn-deficient alloy are in reasonable agreement with earlier measurements of TMR and magnetization. This finding also agrees with the valence band spectra which exhibit a noticeable smearing of the Mn t_{2g} and e_g states for the Mn-deficient alloys. On the other hand, the relative decrease of the measured magnetization, especially the significant violation of the Slater-Pauling rule in the Mn-excessive regime, indicate the presence of additional disorder mechanisms different from the assumed types of antisites disorder. The valence band spectra of the buried $\text{Co}_2\text{Mn}_\beta\text{Ge}_\delta$ thin films exhibit still some major differences compared to stoichiometric bulk Co_2MnGe . However, the electronic structure of the non-stoichiometric films was found to reveal the major characteristic features of the bulk analogue. The observed shift of spectral weight towards the Fermi energy in the non-stoichiometric films compared to bulk Co_2MnGe is in agreement with the changes in the density of states predicted by the calculations. Temperature effects on the states at the Fermi energy that go beyond the broadening of the Fermi-Dirac distributions are not observed. This is, indeed, expected from the high Curie temperature of the compound.

Co-sputtering of Co_2MnGe together with additional Mn is shown to be a well suited technique to tune the stoichiometry of the $\text{Co}_2\text{Mn}_\beta\text{Ge}_\delta$ film composition that provides the possibility to change the electronic structure within the valence band and as a consequence the magnetoresistive characteristics of $\text{Co}_2\text{Mn}_\beta\text{Ge}_\delta$ based tunnel junctions.

ACKNOWLEDGMENTS

The authors thank E. Ikenaga (BL47XU) and S. Ueda (BL15XU) for help with the experiments. This work was funded by the *Deutsche Forschungs Gemeinschaft DFG*

(TP 1.2-A and 1.3-A of the Research Unit ASPIMATT) and the *Japan Science and Technology Agency JST* (DFG-JST project: FE633/6-1). The work at Hokkaido University was partly supported by a Grant-in-Aid for Scientific Research (A) (Grant No. 20246054) from the MEXT, Japan, and by the Strategic International Cooperative Program of JST. The synchrotron radiation HAXPES measurements were performed at BL47XU with the approval of the Japan Synchrotron Radiation Research Institute (JASRI) (Long-term Proposal 2008B0017, 2009A0017) and at BL15XU with the approval of NIMS (Nanonet Support Proposal 2008B4903). The HAXPES experiment at BL15XU was partially supported by the Nanotechnology Network Project MEXT (Japan).

* fecher@cpfs.mpg.de

- ¹ H.-x. Liu, Y. Honda, T. Taira, K. i. Matsuda, M. Arita, T. Uemura, and M. Yamamoto, *Appl. Phys. Lett.* **101**, 132418 (2012).
- ² T. Ishikawa, S. Hakamata, K.-i. Matsuda, T. Uemura, and M. Yamamoto, *J. Appl. Phys.* **103**, 07A919 (2008).
- ³ N. Tezuka, N. Ikeda, F. Mitsuhashi, and S. Sugimoto, *Appl. Phys. Lett.* **94**, 162504 (2009).
- ⁴ T. Ishikawa, H.-x. Liu, T. Taira, K.-i. Matsuda, T. Uemura, and M. Yamamoto, *Appl. Phys. Lett.* **95**, 232512 (2009).
- ⁵ C. Felser, B. Heitkamp, F. Kronast, D. Schmitz, S. Cramm, H. A. Dürr, H.-J. Elmers, G. H. Fecher, S. Wurmehl, T. Block, D. Valdaitsev, S. A. Nepijko, A. Gloskovskii, G. Jakob, G. Schönhense, and W. Eberhardt, *J. Phys.: Condens. Matter* **15**, 7019 (2003).
- ⁶ G. H. Fecher, H. C. Kandpal, S. Wurmehl, J. Morais, H.-J. Lin, H.-J. Elmers, G. Schönhense, and C. Felser, *J. Phys. Condens. Matter* **17**, 7237 (2005).
- ⁷ G. H. Fecher and C. Felser, *J. Phys. D: Appl. Phys.* **40**, 1582 (2007).
- ⁸ T. Block, C. Felser, G. Jakob, J. Ensling, B. Mühling, P. Gütlich, V. Beaumont, F. Studer, and R. J. Cava, *J. Solid State Chem.* **176**, 646 (2003).
- ⁹ T. Block, S. Wurmehl, C. Felser, and J. Windeln, *Appl. Phys. Lett.* **88**, 202504 (2006).
- ¹⁰ K. Inomata, N. Tezuka, S. Okamura, H. Kurebayashi, and A. Hirohata, *J. Appl. Phys.* **95**, 7234 (2004).
- ¹¹ K. Inomata, S. Okamura, A. Miyazaki, M. Kikuchi, N. Tezuka, M. Wojcik, and E. Jedryka, *J.*

- Phys. D: Appl. Phys. **39**, 816 (2006).
- ¹² K. Inomata, M. Wojcik, E. Jedryka, N. Ikeda, and N. Tezuka, Phys. Rev. B **77**, 214425 (2008).
 - ¹³ H. J. Elmers, S. Wurmehl, G. H. Fecher, G. Jakob, C. Felser, and G. Schönhense, Appl. Phys. A **79**, 557 (2004).
 - ¹⁴ H. J. Elmers, S. Wurmehl, G. H. Fecher, G. Jakob, C. Felser, and G. Schönhense, J. Magn. Magn. Mater. **272-276**, 758 (2004).
 - ¹⁵ R. A. de Groot, F. M. Müller, P. G. van Engen, and K. H. J. Buschow, Phys. Rev. Lett. **50**, 2024 (1983).
 - ¹⁶ J. Kübler, A. R. Williams, and C. B. Sommers, Phys. Rev. B **28**, 1745 (1983).
 - ¹⁷ M. P. Raphael, B. Ravel, Q. Huang, M. A. Willard, S. F. Cheng, B. N. Das, R. M. Stroud, K. M. Bussmann, J. H. Claessen, and V. G. Harris, Phys. Rev. B **66**, 104429 (2002).
 - ¹⁸ W. H. Wang, M. Przybylski, W. Kuch, L. I. Chelaru, J. Wang, F. Lu, J. Barthel, H. L. Meyerheim, and J. Kirschner, Phys. Rev. B **71**, 144416 (2005).
 - ¹⁹ Y. Sakuraba, M. Hattori, M. Oogane, Y. Ando, H. Kato, A. Sakuma, T. Miyazaki, and H. Kubota, Appl. Phys. Lett. **88**, 192508 (2006).
 - ²⁰ S. Tsunegi, Y. Sakuraba, M. Oogane, K. Takanashi, and Y. Ando, Appl. Phys. Lett. **93**, 112506 (2008).
 - ²¹ T. Kubota, S. Tsunegi, M. Oogane, S. Mizukami, T. Miyazaki, H. Naganuma, and Y. Ando, Appl. Phys. Lett. **94**, 122504 (2009).
 - ²² M. Oogane, T. Kubota, Y. Kota, S. Mizukami, H. Naganuma, A. Sakuma, and Y. Ando, Appl. Phys Lett. **96**, 252501 (2010).
 - ²³ F. J. Yang, Y. Sakuraba, S. Kokado, Y. Kota, A. Sakuma, and K. Takanashi, Phys. Rev. B **86**, 020409 (2012).
 - ²⁴ S. Ouardi, G. H. Fecher, B. Balke, A. Beleanu, X. Kozina, G. Stryganyuk, C. Felser, W. Kloss, H. Schrader, F. Bernardi, J. Morais, E. Ikenaga, Y. Yamashita, S. Ueda, and K. Kobayashi, Phys. Rev. B **84**, 155122 (2011).
 - ²⁵ P. J. Webster, J. Phys. Chem. Solids **32**, 1221 (1971).
 - ²⁶ G. H. Fecher, H. C. Kandpal, S. Wurmehl, C. Felser, and G. Schönhense, J. Appl. Phys. **99**, 08J106 (2006).
 - ²⁷ P. K. Muduli, W. C. Rice, L. He, and F. Tsui, J. Magn. Magn. Mater. **320**, L141 (2008).
 - ²⁸ P. K. Muduli, W. Rice, C. L. He, B. A. Collins, Y. S. Chu, and F. Tsui, J. Phys. Cond. Mat.

- 21**, 296005 (2009).
- ²⁹ T. Marukame, T. Ishikawa, K.-i. Matsuda, T. Uemura, and M. Yamamoto, *J. Appl. Phys.* **99**, 08A904 (2006).
 - ³⁰ T. Ishikawa, T. Marukame, K. i. Matsuda, T. Uemura, M. Arita, and M. Yamamoto, *J. Appl. Phys.* **99**, 08J110 (2006).
 - ³¹ M. Yamamoto, T. Ishikawa, T. Taira, G.-F. Li, K.-i. Matsuda, and T. Uemura, *J. Phys.: Condens. Matter* **22**, 164212 (2010).
 - ³² S. Hakamata, T. Ishikawa, T. Marukame, K.-i. Matsuda, T. Uemura, M. Arita, and M. Yamamoto, *J. Appl. Phys.* **101**, 09J513 (2007).
 - ³³ T. Taira, T. Ishikawa, N. Itabashi, K.-i. Matsuda, T. Uemura, and M. Yamamoto, *Appl. Phys. Lett.* **94**, 072510 (2009).
 - ³⁴ T. Taira, T. Ishikawa, N. Itabashi, K.-i. Matsuda, T. Uemura, and M. Yamamoto, *J. Phys. D: Appl. Phys.* **42**, 084015 (2009).
 - ³⁵ G. H. Fecher, B. Balke, A. Gloskovskii, S. Ouardi, C. Felser, T. Ishikawa, M. Yamamoto, Y. Yamashita, H. Yoshikawa, S. Ueda, and K. Kobayashi, *Appl. Phys. Lett.* **92**, 193513 (2008).
 - ³⁶ S. Ouardi, B. Balke, A. Gloskovskii, G. H. Fecher, C. Felser, G. Schnhense, T. Ishikawa, T. Uemura, M. Yamamoto, H. Sukegawa, W. Wang, K. Inomata, Y. Yamashita, H. Yoshikawa, S. Ueda, and K. Kobayashi, *J Phys. D: Appl. Phys.* **42**, 084010 (2009).
 - ³⁷ S. Ouardi, A. Gloskovskii, B. Balke, C. A. Jenkins, J. Barth, G. H. Fecher, C. Felser, M. Gorgoi, M. Mertin, F. Schfers, E. Ikenaga, K. Yang, K. Kobayashi, T. Kubota, Oogane, M., and Y. Ando, *J Phys. D* **42**, 084011 (2009).
 - ³⁸ S. Ouardi, C. Shekhar, G. H. Fecher, X. Kozina, G. Stryganyuk, C. Felser, S. Ueda, and K. Kobayashi, *Appl. Phys. Lett.* **98**, 211901 (2011).
 - ³⁹ S. Ouardi, G. H. Fecher, C. Felser, M. Schwall, S. S. Naghavi, A. Gloskovskii, B. Balke, J. Hamrle, K. Postava, J. Pištora, S. Ueda, and K. Kobayashi, *Phys. Rev. B* **86**, 045116 (2012).
 - ⁴⁰ C. Dallera, L. Duo, L. Braicovich, G. Panaccione, G. Paolicelli, B. Cowie, and J. Zegenhagen, *Appl. Phys. Lett.* **85**, 4532 (2004).
 - ⁴¹ G. Panaccione, M. Sacchi, P. Torelli, F. Offid, G. Cautero, R. Sergo, A. Fondacaro, C. Henriquet, S. Huotari, G. Monacof, and L. Paolasini, *J. Electron Spectrosc. Relat. Phenom.* **156-158**, 64 (2007).
 - ⁴² S. Ouardi, G. H. Fecher, X. Kozina, G. Stryganyuk, B. Balke, C. Felser, E. Ikenaga, and

- K. Kobayashi, Phys. Rev. Lett. **107**, 036402 (2011).
- ⁴³ X. Kozina, G. H. Fecher, G. Stryganyuk, S. Ouardi, B. Balke, C. Felser, G. Schönhense, E. Ikenaga, T. Sugiyama, N. Kawamura, M. Suzuki, T. Taira, T. Uemura, M. Yamamoto, H. Sukegawa, W. Wang, K. Inomata, and K. Kobayashi, Phys. Rev. B **84**, 054449 (2011).
- ⁴⁴ T. Ishikawa, T. Marukame, H. Kijima, K. i. Matsuda, T. Uemura, and M. Yamamoto, Appl. Phys. Lett. **89**, 192505 (2006).
- ⁴⁵ S. Picozzi, A. Continenza, and A. J. Freeman, Phys. Rev. B **69**, 94423 (2004).
- ⁴⁶ J. W. Cable and Y. Tsunoda, J. Magn. Magn. Mat. **140-144**, 93 (1995).
- ⁴⁷ H.-L. Luo and P. Duwez, Canad. J. Phys. **41**, 758 (1963).
- ⁴⁸ H. Ebert and M. Battocletti, Solid State Comm. **98**, 785 (1996).
- ⁴⁹ H. Ebert, in *Electronic Structure and Physical Properties of Solids. The Use of the LMTO Method*, Vol. 535, edited by H. Dreysee (Springer-Verlag, Berlin, Heidelberg, 1999) pp. 191–246.
- ⁵⁰ B. Gyorffy, Phys. Rev. B **5**, 2382 (1972).
- ⁵¹ W. H. Butler, Phys. Rev. B **31**, 3260 (1985).
- ⁵² S. H. Vosko, L. Wilk, and M. Nusair, Canad. J. Phys. **58**, 1200 (1980).
- ⁵³ K. Carva and I. Turek, Acta Physica Polonica A **113**, 183 (2008).
- ⁵⁴ C. S. Fadley and D. A. Shirley, Phys. Rev. A **2**, 1109 (1970).
- ⁵⁵ K. Miyamoto, A. Kimura, Y. Miura, M. Shirai, M. Ye, Y. Cui, K. Shimada, H. Namatame, M. Taniguchi, Y. Takeda, Y. Saitoh, E. Ikenaga, S. Ueda, K. Kobayashi, and T. Kanomata, Phys. Rev. B **79**, 1004205(R) (2009).